SEISMIC LOSS AND DAMAGE IN LIGHT-FRAME WOOD BUILDINGS FROM SEQUENCES OF INDUCED EARTHQUAKES

Robert E. Chase[1], Abbie B. Liel[1], Nicolas Luco[2], and Bridger W. Baird[1]
[1]Department of Civil, Environmental, and Architectural Engineering, University of Colorado Boulder, Boulder, CO
[2]United States Geological Survey, Golden, CO

Activities related to oil and gas production, especially deep disposal of wastewater, have led to sequences of induced earthquakes in the central U.S. This study aims to quantify damage to and seismic losses for light-frame wood buildings when subjected to sequences of induced, small to moderate magnitude, events. To conduct this investigation, one and two-story multifamily wood frame buildings are designed, and their seismic response dynamically simulated using three-dimensional (3D) nonlinear models, subjected to ground motion sequences recorded in induced events. Damage is quantified through seismic losses, which are estimated using the FEMA P-58 methodology. Results show that at levels of shaking experienced in recent earthquakes, minor damage, consisting of cracking of interior finishes and nonstructural damage to plumbing and HVAC systems is expected, which is consistent with observed damage in these events. The study also examines how expected losses and building fragility will accumulate and/or change over a sequence of earthquakes. Results indicate that damage quantified in terms of absorbed hysteretic energy tended to accumulate over the sequences; this damage corresponds to elongation or widening of cracks. However, fragility is not significantly altered by damage in a preceding event, meaning structures are not becoming more vulnerable due to existing damage. In addition, sequences of events do not change losses if the building is only repaired once at the end of the sequence, as the worsening of damage does not alter repair actions. If repairs are conducted after each event, though, total seismic losses can increase greatly from the sequence.

KEYWORDS

induced earthquakes, light-frame wood buildings, earthquake sequences, damage accumulation

INTRODUCTION

Activities related to oil and gas production, especially the deep disposal of wastewater, have been responsible for elevated levels of in seismicity in parts of the U.S. In particular, induced seismicity in Oklahoma and southern Kansas has dramatically increased the seismic hazard, *e.g.* [1], and, correspondingly, the risk to infrastructure in the region, *e.g.* [2]. This increase in seismic activity is of concern due to evidence that even relatively small magnitude events can cause damage and economic impacts [3]. The largest event to date in Oklahoma, the September 3rd, 2016, Pawnee earthquake (M_W 5.8), caused damage that included cracking and partial collapse of an unreinforced masonry and brick façade, as well as minor damage to light-frame wood homes [4]. The region experienced a number of smaller earthquakes after the mainshock, including 12 earthquakes with $M_W > 3.0$ in the following month [5].

The induced seismicity observed in Oklahoma and southern Kansas differs from the earthquakes more generally studied by earthquake engineers. In particular, the observed events have been generally of low magnitude (< M_W 5.8 to date), but relatively frequent. Earthquake rates increased substantially from 2009 until 2015, with 888 $M_W \geq 3.0$ earthquakes occurring in 2015, compared to only 130 experienced in California in the same year [6]. More recently, earthquake rates have decreased somewhat, with over 400 $M_W \geq 3.0$ earthquakes in Oklahoma in 2017 and around 200 in 2018 [6, 7]. Unlike tectonic events, these earthquakes typically occur in swarms, *i.e.* seismic sequences where multiple earthquakes occur in a short time frame [8, 9]. These sequences occur due to the migration of injected fluids and associated pore water pressures and static stresses along already critically stressed faults. In addition, much of the building stock is older, and even modern buildings were designed for much lower levels of seismicity than those recently observed [10, 11]. The response of buildings and infrastructure in low to moderate magnitude earthquake sequences, and the potential for damage accumulation, is not well understood.

Yet, a recent survey of 233 Oklahoma homeowners in affected regions found that 43% of those surveyed have reported some amount damage from induced earthquakes, with 18% reporting damage costing $1000 or more [12]. 33% of those surveyed reported that they believed their residences experienced accumulated damage over multiple earthquakes. Homeowner and activist groups have also asserted that damage is accumulating in these series of smaller earthquakes more than might be expected, expressing concerns about each earthquake increasing vulnerability of the structure in subsequent events [13]. For example, one respondent to the U.S. Geological Survey ‘Did you feel it?’ site wrote “The cracks just keep getting bigger… They are destroying my house little at a time” [14]. Another resident stated: “I’m worried the next one would bring my house down on top of me” [15]. Insurers have also acknowledged that “accumulation of loss from property…. for earthquake scenarios” is now a “realistic possibility” [16].

This study aims to quantify damage to and seismic losses for light-frame wood buildings when subjected to sequences of smaller magnitude events. Three research questions are investigated: 1) what damage can we expect in light-frame wood buildings in induced earthquakes? 2) how does this damage change if the building experiences an earthquake sequence? 3) are these results consistent with observations from Oklahoma to date? To address these questions, one and two-story multifamily wood frame buildings are designed, and their seismic response dynamically simulated using nonlinear models subjected to recorded ground motion sequences from induced earthquakes. Damage is quantified through seismic losses, which are estimated using the FEMA P-58 methodology [17], in order to assess damage and losses to the building even when damage to the structural system itself may be limited. To address the impact of earthquake sequences, we also examine how expected losses and building fragility may accumulate and/or change over a sequence of earthquakes, and compare damage observed in past events to the simulation results.

LITERATURE REVIEW

Effect of Induced Earthquakes on Buildings and Infrastructure

Research has shown that induced seismicity increases seismic hazard, and that this increase can be meaningful in the range of ground shaking intensities that matter for building response. For example, Petersen et al. [18] show a 130-fold increase in likelihood of shaking of Sa(T=0.5s) > 0.25g for Edmond, Oklahoma, compared to a seismic hazard forecast that excludes induced seismicity. This model suggests the likelihood of higher magnitude events, up to about M_W 7, and hence, higher shaking levels, is low, but still present. Another study using a different hazard model also found an elevated seismic hazard for the region [19]. Similar trends have been observed elsewhere for induced seismicity associated with hydraulic fracturing and gas production [20, 21]. By convolving the hazard model from Petersen et al. [1] with assumed fragility models for collapse and the threat to life safety from falling hazards, Liu et al. [2] found that this increased seismic hazard also elevated these risks substantially compared to the baseline natural seismicity.

There have been relatively few studies examining the fragility and response of buildings in induced earthquakes, likely because of the relatively small magnitude of the events experienced. Chase [23] found that, for brittle structures such as residential brick chimneys, induced motions were somewhat less damaging when compared to similar tectonic records for a given spectral intensity. However, this difference appears to stem largely from differences in motion frequency content, influenced by depth and tectonic region. Hence, they concluded that a larger magnitude induced earthquake could have similar impacts to a tectonic event in the same region. Potential damage to bridges in Oklahoma and Texas has also been investigated. Harvey et al. [24] concluded that slight to moderate damage is possible to bridges in induced earthquakes. Khosravikia et al. [25] developed fragility curves for different damage states for Texas bridges subjected to both induced and tectonic motions. The study found that there was a greater chance of experiencing slight or moderate damage in Texas bridges when induced seismicity is considered in the hazard model.

Seismic Response of Light-Frame Wood Buildings

Light-frame wood construction comprises the majority of the building stock across the United States. Historically, light-frame wood buildings have performed well in earthquakes with a relatively low risk of catastrophic collapse and life endangerment [26]. However, there is potential for significant seismic losses; the 1994 Northridge Earthquake caused an estimated property loss of $20 billion to light-frame wood construction alone (in 1994 dollars) [27].

In part as a response to this damage, there have been a number of large efforts, *e.g.* [28, 29], to improve understanding of and quantify the seismic response of these structures. In the NEESwood project, Van de Lindt et al. [30] tested a full-scale six-story light-frame wood residential building with nonstructural finishes (e.g. gypsum wallboard) on a shake table. The building was designed according to a new displacement-based approach. Damage was observed in the form of cracks to the gypsum wallboard, but no structural damage was experienced, even at the maximum considered earthquake (MCE) level. Filiatrault et al. [31] showed that it is critical to incorporate the effects of nonstructural components in seismic performance assessments of these buildings, as they can significantly change the expected stiffness, strength, and fundamental period of the building. Christovasilis et al. [32] conducted incremental dynamic analysis on modern, seismically designed wood frame buildings to investigate their collapse performance at the MCE level. That study showed that, in addition to wall finish materials, construction quality and excitation direction can significantly affect the assessed collapse fragilities. More recently, projects such as the Applied Technology Council (ATC) 116 [33, 34], have investigated the performance of many short period structures, including light-frame wood construction, in areas of high seismic hazard. That study shows that light-frame wood buildings have good collapse resistance.

Analytical tools have also been developed from experimental testing, through the CUREE Caltech Woodframe Project and the NEESWood Capstone Test and others [35] [36]. SAPWood [37] and Timber3D [38] build on capabilities of previous models with nonlinear shear wall elements with model parameters calibrated to experimental testing results. These tools capture the hysteretic response of the shear walls and large deformations of near collapse level response, and have shown reasonable agreement with the response of light-frame wood buildings in full-scale shake table tests [37].

Damage Accumulation

Earthquake engineering performance assessments are often based on the assumption that the building is in an undamaged state when an earthquake occurs. However, in cases of seismic swarms and mainshock-aftershock sequences, there may not be enough time for retrofit or repair of the structure before the next shaking event, and, as a result, the building's damage and response may be influenced by what happened in a preceding event. There are some documented historical cases in which a building withstood an initial larger magnitude earthquake only to collapse in a smaller magnitude at a later time attributed to this phenomenon [39, 40].

Structural damage accumulation has been a topic of research for many years. Ballio and Castiglioni [41] and Amadio et al. [42] examined the effect of multiple earthquake loadings on linear and nonlinear numerical models of single-story steel structures and single-degree-of-freedom structures, respectively. Both studies quantified damage using a q-factor (ductility) and compared ductility demand as a function of earthquake loading characteristics, finding that damage accumulation was greater for systems with higher deformation capacities. More recently, Ghosh et al. [43] developed a probabilistic framework for assessing damage accumulation in highway bridge columns, using the Park & Ang [44] damage index. The study found that there was a significant increase in damage index exceedance probabilities within each scenario's time frame when multiple events were considered.

Focusing on damage accumulation in mainshock/aftershock contexts, Jalayer & Ebrahimian [45] investigated cumulative damage in reinforced concrete (RC) buildings, considering the time-dependent rate of aftershock occurrence. The study found significantly higher risks of damage when considering a structure damaged initially by a mainshock than a mainshock alone. In addition, Hatzigeorgiou and Liolios [46] examined the impact of mainshock-aftershock sequences on RC frame structures. That study observed more damage from earthquake sequences, compared to single events of the same ground motion intensity. Likewise, Raghunandan et al. [47] examined multiple RC moment frame structures designed to current code standards subjected to mainshock-aftershock sequences. Their work showed that collapse capacity of a structure was not significantly influenced if a mainshock did not significantly damage the structure. However, if the building was extensively damaged in the mainshock, the collapse capacity dropped significantly. These findings have been confirmed by others, *e.g.* [48, 49]. Simulations by Shokrabadi and Burton [49] also examined RC frames, showing that a mainshock can decrease a structure's ability to remain occupiable in a subsequent event. Looking specifically at the light-frame wood buildings of interest here, Nazari et al. [50] simulated response of a two-story residential building, subjected to artificial mainshock-aftershock sequences. They showed that the structure's fragility increased when subjected to multiple seismic pulses, but not to the extent that has been observed with other studies focusing on other structure types (*i.e.,* steel or RC). Goda and Salami [51] also investigated mainshock-aftershock sequences on light-frame wood construction, showing that aftershocks were associated with a 5–20 % increase of the median inelastic seismic demand curves when the structure was already in a moderate damage state.

These results show that damage accumulation in earthquake sequences can influence damage and seismic loss. Seismic loss has been identified as the key seismic performance measure for light-frame wood construction. This study aims to investigate the performance of light-frame wood buildings in sequences of induced earthquakes.

GROUND MOTION SELECTION

This study incorporates recorded ground motions from confirmed induced earthquakes in Oklahoma and southern Kansas for dynamic analysis. These ground motions are obtained from the Rennolet et al. [52] database, which includes more than 300,000 motions. These motions were filtered and processed according to recommendations of NGA-West2 [53]. Real seismic sequences are selected to better capture the effects of these earthquakes on buildings. In particular, Ruiz-Garcia and Negrete-Manriquez [54] found that mainshock-aftershock studies using synthetically-created sequences can overestimate the damage observed from the multiple motions because the frequency content is not realistic.

For engineering analysis, we were interested in identifying the highest intensity records that form two or three motion sequences in this dataset. To do so, first, the records in the database with the highest geometric mean of peak ground acceleration in the two orthogonal directions (or PGA) are selected as targets. For each of these records, a time window of 15 days before and after is defined. All earthquakes within this time window and with an epicenter within a 25 km radius of the event producing the target record are then considered for selection of motions to form a sequence. These temporal and spatial constraints are intended to ensure that these sequences are consistent with the observed seismicity, but we place no restrictions on the recording station being the same to ensure we obtain records of interest for engineering analysis. The two records with the largest earthquake magnitudes (and if records were from the same magnitude earthquake, the largest PGA) in the window are then combined with the first target record to create a three-record sequence, maintaining the same order as the events occurred. There is no overlap of motions between different sequences. In total, 19 sequences, each comprised of three motions, are selected for 57 total motions, with each motion having two horizontal components.

Figure 1 summarizes the ground motion suite characteristics. For the entire ground motion set, the median earthquake magnitude is M_W 3.5, the median PGA is 0.10 g, and the median significant duration (5-95% Arias Intensity) is 1.9 seconds. *SaRatio*, which quantifies spectral shape [55] as a ratio of the spectral acceleration (Sa) at a period of interest, divided by the average Sa over a period range, is shown for two period ranges: 0.3s to 0.9s and 0.5s to 1.5s.

BUILDING ARCHETYPES AND DESIGN

The one and two-story building archetypes analyzed here are chosen to be representative of the typical multifamily residential building stock in the Oklahoma region. The buildings examined in this study were originally designed in accordance with ASCE 7-10 [11] for "moderate seismicity" for the ATC 116 project by that project team [33, 34]. There, "moderate seismicity" refers to locations at the upper limit of seismic design category (SDC) C, referred to as "C_{max}", and corresponding to a short-period response acceleration parameter (S_{DS}) of 0.50g [11, 56]. Oklahoma and southern Kansas fall in SDC B, so we redesigned the buildings for a location in Edmond, OK with S_{DS} of 0.26g according to ASCE 7-16 using the same wall layouts (for both shear walls and nonstructural partitions) as the original models. In the redesign, shear wall lengths were decreased and nail spacing was increased to reduce the building strength. In addition, we compared design wind forces for the site to the SDC B seismic forces, and seismic forces controlled.

The design of each multifamily residence covers a 14.6 m by 29.3 m (48 ft by 96 ft) footprint. This design accommodates six 7.3 by 9.8 m (24 ft by 32 ft) apartment units in the one-story building, as shown in Figure 2 and Figure 3. The layout of shear walls in the two-story archetype accommodates four two-story 7.3 m by 14.6 m (24 ft by 48 ft) townhouses; see [63] for a diagram. The exterior walls for both archetypes are framed with 5cm x 15 cm (2 in x 6 in) lumber and have OSB sheathing. The exterior faces are clad in siding. We assumed James Hardie type siding, which is the most common finish material in Oklahoma [57]. This decision is important, as finishes and siding materials can have a pronounced impact on the seismic response of the structure [31]. The interior face of the exterior walls is clad with 1.3 cm (0.6 in) gypsum wallboard. The interior shear walls (party walls) are actually two lines of 5x10 cm (2 in x 4 in) framing separated by a 2.5 cm (1 in) gap, which would in reality be a larger corridor, finished with gypsum wallboard on the face of the wall toward the interior of the unit, but with no sheathing applied to the corridor face, to represent typical framing. The foundation for both archetypes is a 5 cm (4 in) concrete slab on grade, with spread footings at the interior posts and reinforced grade beams integral with the slab at the perimeter and along all interior load bearing walls. For the 2-story archetype, the floor system is framed with 5 cm x10 cm (2 in x 4 in) in parallel chord trusses, spaced at 61 cm (24 in) on center.

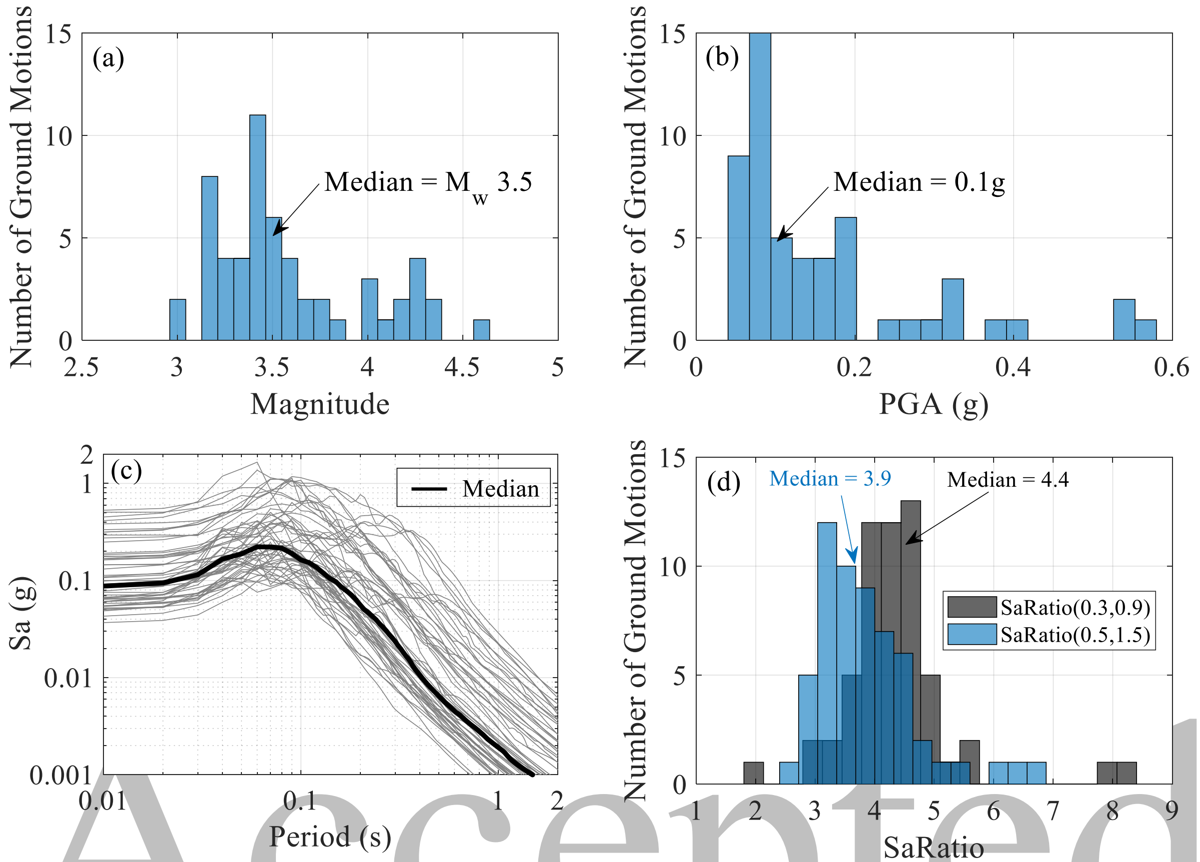

Figure 1. Ground motion characteristics for 57 selected induced motions showing a) earthquake magnitudes, b) geomean PGA, c) geomean acceleration response spectra, and d) *SaRatios* for two period ranges, *i.e. SaRatio(0.3,0.9)* and *SaRatio(0.5,1.5).*

BUILDING MODELING

The buildings are modeled using Timber3D, a nonlinear structural analysis software for wood frame construction based in MATLAB and developed by Pang et al. [38, 58]. The software is intended for three dimensional (3D) simulations of seismic responses of light-frame wood buildings, representing individual wood frame elements and the interaction of their responses. Timber3D is capable of providing estimates of collapse level horizontal and vertical displacements. Timber3D improves upon the so-called lumped parameter approach *SAWS* [36] and *SAPWood* [59], by employing a finite element methodology with nodal condensation to decrease the required computational energy. In addition, Timber3D is formulated to capture vertical uplift forces present in light-frame wood shear walls, as well as large displacements in flexible diaphragms. The goal of this study is to simulate seismic response of wood light frame buildings and to examine the sensitivity of response to sequences of earthquakes, i.e. effects of multiple loading cycles. Thus, it is particularly important to capture cyclic and in-cyclic degradation to quantify loading cycle effects [60, 61, 47, 42]. It is also important to capture large deformations and geometric (P-delta) effects, *e.g.* [62], in order to simulate sidesway collapse in the first story, the predominant failure mechanism in light-frame wood buildings [38, 63]. These models are adapted from models from those used in ATC 116, which were provided by Ziaei Ghehnavieh [63].

In these models, nonlinear behavior is modeled only in the wall elements. Wall elements include both the shear walls, which in the design are taken to be the sole lateral force resisting system, and the interior (nonstructural) partition walls. Figure 4(a) and (b) show the hysteretic characteristics for 1.2 m by 3 m (4 ft by 10 ft) sections of an exterior shear wall and interior shear wall, respectively, illustrating the model's treatment of strength and stiffness deterioration, in-cycle and cyclic deterioration, and pinching effects. These hysteretic plots show the nonlinear response for the wall without any nonstructural finishes, the effect of which are shown separately in Figure 4(c) for the exterior (James Hardie) siding. In Timber3D, these elements are assigned at the same location such that the composite wall response accounts for structural and nonstructural contributions. The hysteretic model that defines the response of the nonlinear wall elements and finishes (except for the siding) is a modification to the Modified Stewart Hysteretic Model [63]. The model parameters for each individual wall element represents cyclic wall behavior as a function of wall length, and nail and stud spacing, and were calibrated by Ziaei Ghehnavieh [63] to experimental results. Details of the parameters used for each material type, including the residual strength of 0.30, are taken from and provided in [63]. The Modified Stewart Hysteretic Model was developed based on experimental testing of wood shear walls under quasi-static loading [35]. The modified model [63] employed here follows the same hysteretic behavior, but fits an "S" curve to the post peak response, instead of a linear degradation, to capture nonlinear strength decay and better represent residual strength observed at large displacements in wood-frame shear walls [63]. Difference between the two models can be observed by comparing Figure 4(a) and Figure 4(c). Siding (Figure 4(c)) was modeled using the original Modified Stewart Hysteresis Model.

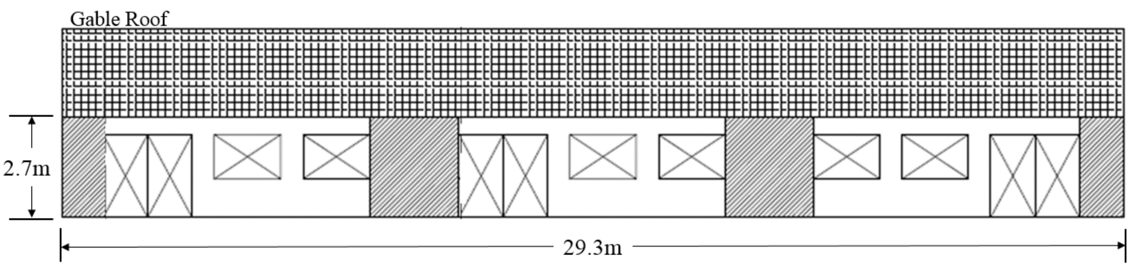

Figure 2. Elevation view of the one-story multifamily wood frame building (image modified from [33]**).**

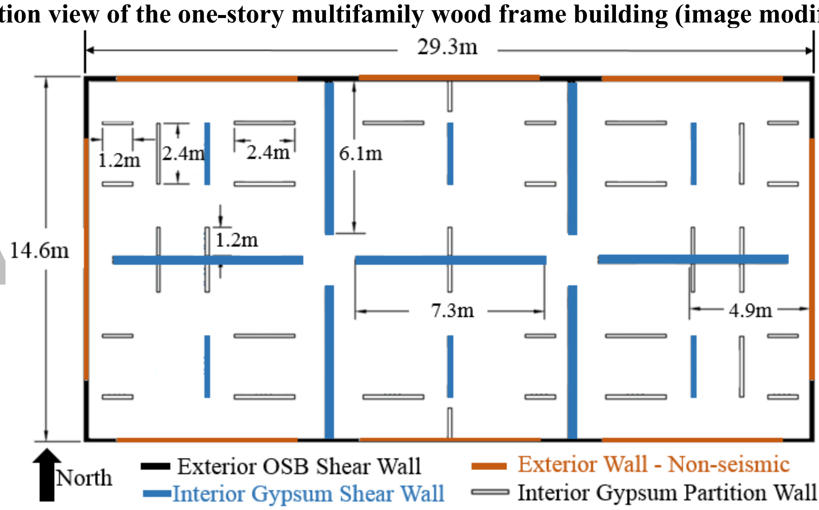

Figure 3. Plan view of the one-story multifamily wood frame building (image modified from [33]**). The exterior OSB shear walls correspond to OSB-Low in** [63]**, and the interior shear walls correspond to Min-Gyp in** [63]**.**

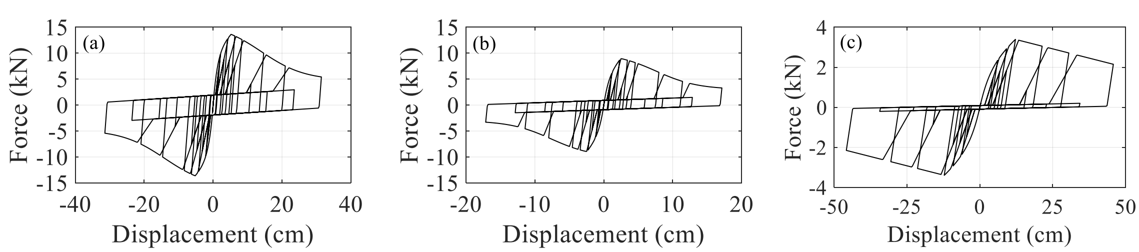

Figure 4. Force vs. displacement hysteresis of 1.2 m wide by 3 m tall (4 ft by 10 ft) sections of a) an exterior OSB shear wall, b) an interior gypsum shear wall, and c) nonstructural exterior siding found in the one and two-story buildings. Calibration of component models from [63]**.**

The concrete foundation, sill plates, stud elements, and floor diaphragms are modeled as elastic elements, while the hold downs and anchor bolts are modeled to be rigid; soil response is not modeled. Koliou et al. [64] showed that modeling the diaphragm flexibility of a single-story wood-frame structure was essential in accurately capturing some buildings' responses in terms of drifts and accelerations. In this study, the diaphragms are modeled to be elastic, but rigid (consistent with ATC 116). The base of the structure is modeled as effectively fixed.

Timber3D's formulation captures large geometric deformations and corotational effects, which together with modeling of hold down and contact forces between the framing members [58], enables simulation of large vertical displacements as sidesway collapse occurs. We define collapse by the downward (vertical) displacement of the second floor exceeding 25 cm (10 in). Results are not very sensitive to the exact definition of vertical displacement corresponding to collapse as, at this point, lateral and vertical displacements are increasing without bound.

The fundamental periods of the one and two-story buildings are 0.29 and 0.45 seconds, respectively. In accordance with other previous studies, *e.g.* [58, 37], we applied 1% Rayleigh damping (initial stiffness). This damping is applied at the fundamental modes in both the E-W and N-S directions, and represents elastic damping and ensure that movement of the structure from the first motion in the sequence dies out before the next ground motion was applied. Sensitivity analyses demonstrated that nonlinear response and collapse capacities were not very sensitive to assumed damping, indicating that formulation adopted herein avoided overdamping when combined with hysteretic damping in the nonlinear range of response.

Figure 5 compares the pushover curves for both buildings, compared to the design base shear. The design base shears differ in the two directions because OSB shear walls (R = 6.5) comprise the lateral force resisting system in the E-W direction and gypsum shear walls (R = 2) govern the N-S direction [11]. The two-story building is stronger than the one-story building, but also somewhat less ductile. For both buildings, and in both directions, the ultimate strength of the building is much higher than the design base shear, due to the contribution of nonstructural partition walls and finishes in the models.

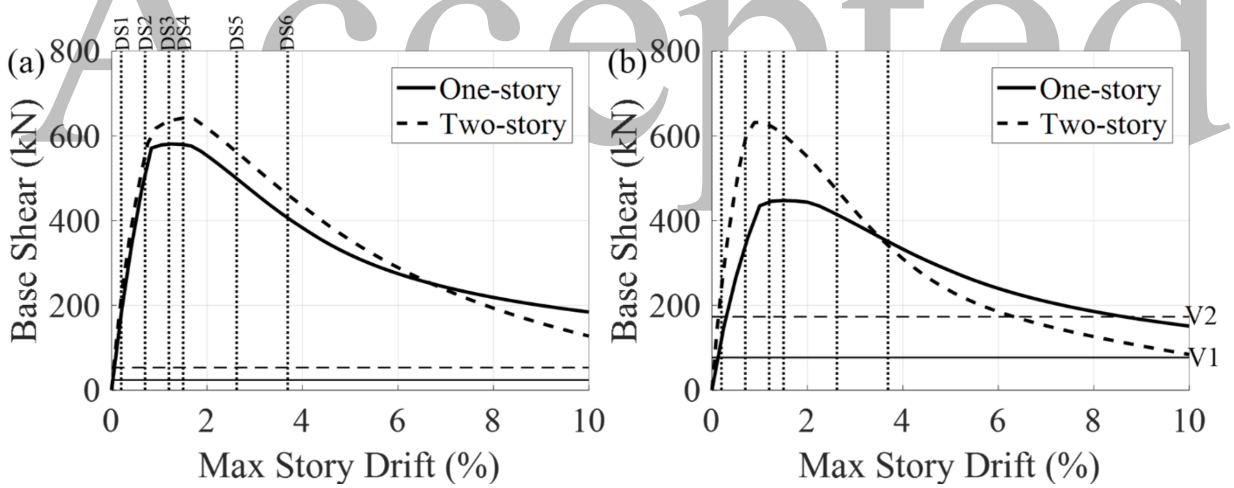

Figure 5. Pushover curves for the one and two-story buildings in a) E-W direction and b) N-S direction. Drifts corresponding to the global damage states are labeled in (a), and described in more detail in Table 1. V1 and V2 in (b) represent the design base shear for the one and two-story buildings.

DAMAGE ASSESSMENT METHODOLOGY

Damage and Loss Definitions

We define damage as any seismic loss. Structural damage is associated with losses to structural components, *i.e.* interior and exterior shear wall elements. The nonstructural components consider damage to partition walls, and electrical, HVAC, and plumbing systems. Direct seismic loss, defined as seismic repair costs, is quantified using the Seismic Performance Prediction Program (SP3) [65]. SP3 adopts the FEMA P-58 [17] methodology to organize building fragilities, component fragilities, population information, and other inventories to estimate the losses. This methodology is probabilistic and involves many (in this case, 1000) realizations of structural response, propagated through damage and repair models that consider correlations in component in building response.

Damage in Single Event

To quantify damage in induced earthquakes, we first run all 57 individual motions in an incremental dynamic analysis (IDA) [66] of the undamaged buildings. In IDA, each record is scaled up by increasing the spectral acceleration at the fundamental period of the structure, $Sa(T_1)$, and rerunning the motion until collapse occurs. The peak story drift ratios (SDR), floor accelerations, and residual drifts are recorded at nine nodes at each floor to capture torsional effects. In this 3D analysis, the intensity measure (IM) is the maximum $Sa(T_1)$ of the two components of each record. We randomly assign one of the motions to the N-S direction of the building, and the other to the E-W. A one-second cushion of zero acceleration was added to the end of each ground motion, and residual drifts were calculated as the average over that time; although the building does not come to rest completely after 1 sec, we confirmed that this approach provided good estimates of residual drifts.

Damage in Sequence of Events

To explore how damage and seismic loss occur in sequences of motions, we create artificial sequences from the recorded ground motions with different scaling combinations, as illustrated in Figure 6. For each sequence, the first motion is scaled such that the building just reaches damage state (DS) *i*. These DSs are defined to correspond to different story drift ratios (SDR), as shown in Figure 5, similar to *e.g.,* [47]. The definitions of these DSs, provided in Table 1, are taken from FEMA P-58 [17], and correspond to the median SDR at which various types of damage occur in the two shear wall types that are present in these buildings. The DSs are used solely to define the scale levels for the first motion in the sequence.

Table 1. Definition of global damage states used in scaling records in sequences.

Damage State	SDR (%)	Qualitative Description
DS1	0.2	Screws popping out, minor cracking of wallboard, warping or cracking of wallpaper in OSB shear walls
DS2	0.7	Moderate cracking or crushing of gypsum finishes in OSB shear walls (typically in corners and in corners of openings)
DS3	1.2	Significant cracking and/or crushing of gypsum finishes on OSB shear walls and buckling of studs and tearing of tracks
DS4	1.5	Slight separation of sheathing or nails that come loose in gypsum shear walls
DS5	2.6	Permanent rotation of sheathing, tear out of nails or sheathing in shear walls
DS6	3.7	Fracture of studs, major sill plate cracking in shear walls

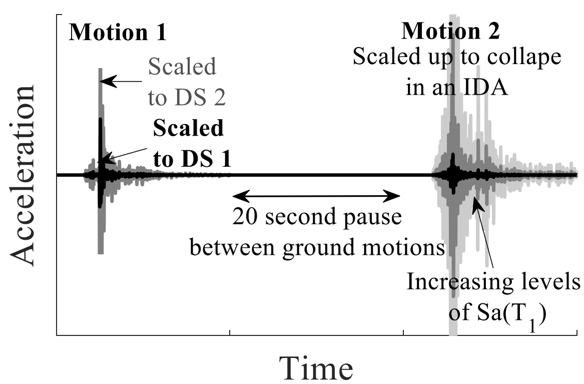

Figure 6. Illustration of sequences of two motions, showing scaling of motion 1 to a DS of interest, and the IDA applied to motion 2.

The first scaled motion is combined with a second motion that is scaled in an IDA to create a sequence, with a 20 second buffer between the motions to allow the structure to come to rest. The second motion in the sequence is scaled by $Sa(T_1)$ as described above, creating a family of sequences, each reaching the same DS in motion 1, but with different scale factors on motion 2.

We also created some three-motion sequences, following a similar procedure to that shown in Figure 6. In this case, the first motion is scaled such that the building just reaches DS *i*. The second motion is scaled such that the building just reaches DS *i+1*. The third motion is scaled through IDA, and 20 second pauses are added between the motions. Only the two-story building was subjected to the three-motion sequences. For the two-story building, results were very similar for the two and three-motion sequences (discussed below). For this reason, only the single and two-motion sequences were applied to the one-story building.

Hazard Consistent Adjustments to Structural Response

One shortcoming of IDA is the bias that can result from scaling ground motions above the level at which they were recorded, producing ground motions that are inconsistent with the hazard and have unrealistic frequency content [66, 67]. This presents a difficulty here, because of our interest in examining earthquakes and ground motions beyond the levels that have been experienced. Although multiple approaches exist to address this limitation, recently, Chandramohan [68] developed a framework that can produce hazard consistent results while using a generic set of ground motions in an IDA. In this methodology, hazard consistent measures of spectral shape and ground motion duration are used to adjust the results of a generic IDA to represent realistic ground motion characteristics. We employ this framework here to adjust engineering demand parameters or EDPs (namely, SDR, floor accelerations, residual drifts and collapse capacities) obtained from the IDA to account for the expected spectral shape at a typical Oklahoma site. We adjust EDPs to account only for spectral shape, which is quantified the dimensionless parameter, *SaRatio* [55]; we do not account for ground motion duration because this parameter was not found to be critical for the EDPs of interest [22]. *SaRatio* is defined as $Sa(T_1)$, normalized by Sa_{avg}, where Sa_{avg} is the average of the spectral accelerations across a range of periods [55]. Although Eads et al. [55] recommend a period range of $0.2T_1$ to $3T_1$, we instead use T_1 to $3T_1$ because higher modes (*i.e.* $T < T_1$) are not important for our short period buildings of interest. A higher *SaRatio* indicates a more peaked spectrum at the T_1 of interest. A ground motion with a lower *SaRatio* is often more damaging to a structure. *SaRatio* is a convenient measure of spectral shape because it can be computed using standard Sa-based ground motion prediction equations (GMPE).

The hazard consistent IDA methodology involves, first, quantifying the expected spectral shape at a site of interest, and then adjusting the generic IDA results to be consistent with that expected shape [68]. To quantify the expected spectral shape, we examine the deaggregated hazard [69] from the USGS's 2018 one-year forecast, which includes induced seismicity, for Edmond, Oklahoma. This deaggregation information includes moment magnitude (M_w), shortest distance from the site to the fault plane (R), and percent contribution for different earthquake scenarios at nine different hazard levels of interest at Sa(T=0.3s) and Sa(T=0.5s), quantified by the geometric mean of the horizontal components. The deaggregation also reports epsilon (ε), defined as the number of standard deviations by which an observed logarithmic *Sa* differs from the mean logarithmic *Sa* from a GMPE. For hazard deaggregation only, we assume site conditions are at the boundary between site class B and C (V_{s30} = 760 m/s). At each hazard level, we calculate hazard consistent target *SaRatios* from the deaggregated hazard for each building at multiple hazard levels following [68], and the Atkinson [70] GMPE.

Table 2 shows the calculated target *SaRatio* and associated $Sa(T_1)$ for each hazard level for the one and two-story buildings. These results show that the expected spectral shape is very peaked in Edmond (as indicated by *SaRatios* >> 2); for comparison, typical expected shapes in San Francisco at the same periods would be associated with *SaRatio(0.3,0.9)* = 2.1 and *SaRatio(0.5,1.5)* = 2.4 for the 2475 year return period. This peaked shape stems from the high values of epsilon obtained from hazard deaggregation. In these deaggregations, the expected magnitudes and distances do not change significantly with different hazard levels. Instead, the hazard at longer return periods is driven by variability in the ground motion, and more and more rare motions from these events (quantified by epsilon). The mean *SaRatio(0.3,0.9)* of all 57 induced ground motions is 4.4 for the one-story building and the mean *SaRatio(0.5,1.5) is* 3.8 for the two-story building, as shown in Figure 1(d). In general, the target *SaRatio*s (either *SaRatio(0.3,0.9)* or *SaRatio(0.5,1.5)*) are larger than the median SaRatios of the record set (with exception of the 75 and 275 year return periods). This trend indicates that the records used in the IDA are less peaked (more damaging) than anticipated for Edmond based on the hazard deaggregation.

We also ran the generic IDA with the FEMA P-695 Far-Field set [56], consisting of 22 pairs of records, and combined the results with the 57 motions from induced events. The FEMA Far-Field set has a range of *SaRatio(0.3,0.9)* of 0.9 to 2.5 and *SaRatio(0.5,1.5)* of 1.1 to 4.5. These records with lower *SaRatio* were analyzed to provide a broader range of *SaRatio* to inform trends of structural response versus *SaRatio*.

The hazard consistent IDA approach adjusts EDPs of interest from the generic IDA to the target *SaRatios* using regression analysis [71]. Specifically, a linear regression analysis is carried out between each EDP (at each hazard level) in natural logarithmic space between the EDP and *SaRatio* for the motions used in the IDA, as shown in Figure 7(a). The results of this regression, illustrated in Figure 7(b), are used to produce a median EDP prediction that is conditioned on the target *SaRatio* at each hazard level. An example of the regressions for several hazard levels and their associated adjustments is shown in Figure 7(b). The solid dots on each line in Figure 7(b) show the target *SaRatio(0.3,0.9)* and corresponding hazard consistent EDP for that hazard level. We carried out this regression for three EDPs in each of the two directions (SDRs for each story, residual drifts, and collapse capacities) at 9 hazard levels, for both buildings.

Table 2. Deaggregated hazard information, and associated Sa(T_1) and *SaRatios* at periods corresponding to one-story and two-story buildings.

	One-Story Building					Two-Story Building				
Hazard Level* [1/yr]	**Mean M_W**	**Mean R [km]**	**Mean ε**	**Sa(T_1=0.3 s) [g]**	**Median Target *SaRatio (0.3,0.9)***	**Mean M_W**	**Mean R [km]**	**Mean ε**	**Sa(T_1=0.5s) [g]**	**Median Target *SaRatio (0.5,1.5)***
$1.3x10^{-2}$	5.7	16.8	0.7	0.51	4.1	5.9	21.7	0.6	0.27	3.7
$3.6x10^{-3}$	5.8	13.8	1.1	0.97	4.5	6.0	16.0	1.0	0.51	3.8
$2.1x10^{-3}$	6.0	13.1	1.1	1.2	4.6	6.1	14.6	1.0	0.65	3.9
$1.0x10^{-3}$	6.0	12.4	1.3	1.6	4.8	6.2	14.2	1.2	0.88	4.1
$4.0x10^{-4}$	6.1	10.8	1.6	2.2	5.1	6.3	12.3	1.4	1.2	4.4
$2.5x10^{-4}$	6.2	10.9	1.6	2.5	5.3	6.4	12.1	1.5	1.5	4.7
$1.6x10^{-4}$	6.2	10.4	1.7	2.8	5.6	6.5	12.6	1.6	1.7	4.9
$1.2x10^{-4}$	6.2	10.3	1.8	3.0	5.8	6.5	12.5	1.7	1.8	5.0
$1.0x10^{-4}$	6.3	10.2	1.9	3.2	5.9	6.5	12.4	1.7	1.9	5.2

*Quantified by annual rate of exceedance

Floor accelerations were not adjusted to be hazard consistent. Our results showed that correlations between floor accelerations and *SaRatio* are very low. These poor correlations occur because the peak accelerations from the induced records occur early in the time history, in the first few seconds of strong shaking, when the building is still elastic, due to the short duration and pulse-like characteristics of these motions, such that floor accelerations are not dependent on spectral shape. Interestingly, peak floor accelerations in the longer duration FEMA Far-Field motions occurred at different points throughout the time history, sometimes after the structure had entered the nonlinear range, showing more dependency on *SaRatio*.

We also quantify the uncertainty in the obtained EDP, considering the record-to-record variability, *i.e.* the uncertainty in the regression as described in [68, 71].

The median IDA curves from the 1^{st}-story drift for the one and two-story buildings are shown in Figure 8. In both buildings, the hazard consistent drifts are less than the directly simulated drifts for a given intensity. This trend occurs because the target *SaRatio* at almost all hazard levels is greater than the median *SaRatio* of the record set used in the IDA. The more peaked a spectrum is expected to be (higher *SaRatio)*, the lower the estimated drifts.

For loss assessment, SP3 takes as input a vector of structural analysis results for each hazard level and EDP of interest. This vector traditionally includes the structural response results for each ground motion run in the analysis. Here, the median EDP and standard deviation are used to produce multiple EDP realizations for each hazard level for input into the Monte Carlo simulation; in this study, we did not consider correlations in these realizations, but have shown these correlations have little effect on mean losses.

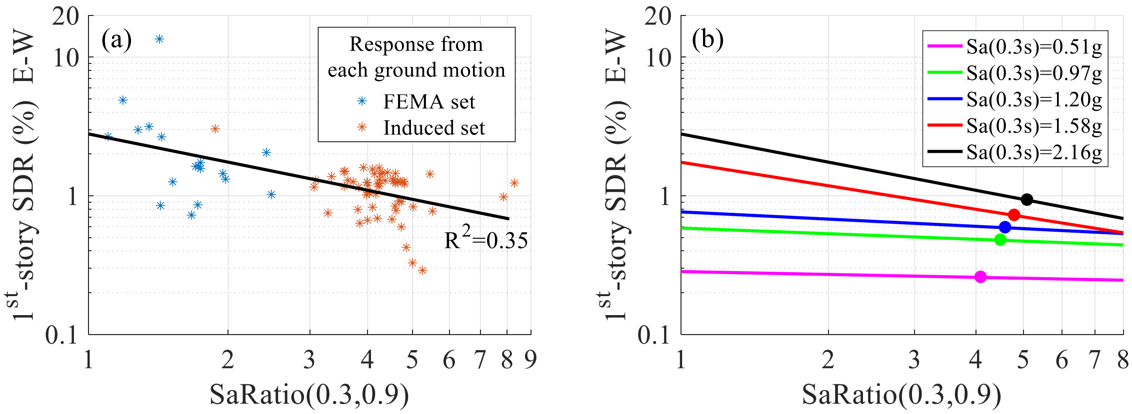

Figure 7. Illustration of hazard consistent IDA adjustment for the one-story building showing a) regression between 1st-story SDR and *SaRatio* at the 2475 year hazard level [*Sa(0.3s)*=2.16g], and b) regressions for the same EDP at five different hazard levels (annual rates of exceedance from 1.3 x 10^{-2} to 4.0 x 10^{-4}). Solid dots in (b) show the target *SaRatio(0.3,0.9)* and corresponding hazard-consistent EDP for each hazard level.

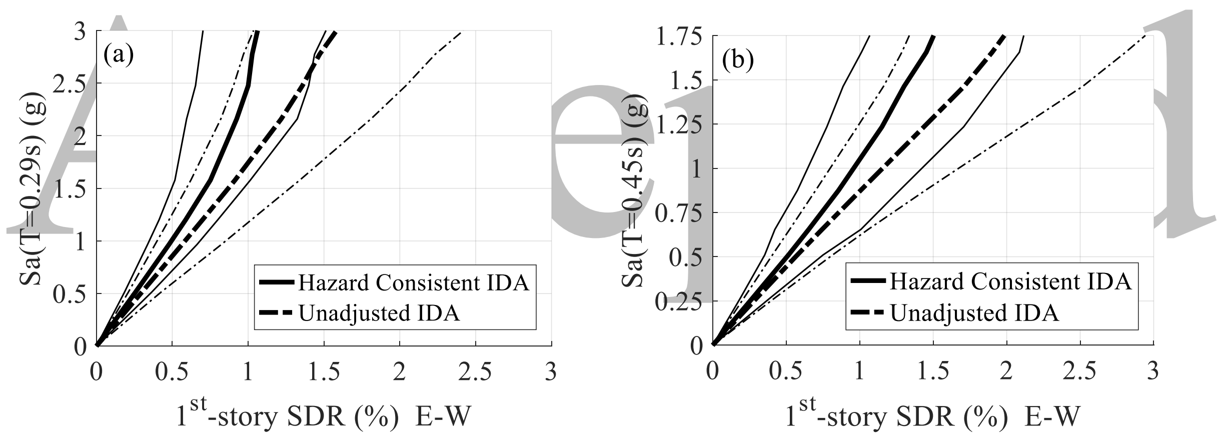

Figure 8. Median ± standard deviation 1st-story SDRs comparing original (unadjusted) and hazard consistent IDA results for the a) one-story and b) two-story buildings.

DAMAGE TO BUILDINGS IN A SINGLE EVENT

Figure 9(a) shows the total expected seismic loss for the one-story building, normalized by the replacement cost of the building, for both the unadjusted and hazard consistent IDAs. For the purpose of the normalization, the total replacement cost is taken to be approximately \$170/ sq ft. for either building, corresponding to \$790,000 for the one-story building, and excludes the cost of demolition. Figure 9(b) breaks down this total loss by component category for both analyses. The shear walls had the highest contribution to losses at all intensity levels. This damage sustained by shear walls is characterized by cracking of the gypsum or OSB wallboard at lower intensity levels, and fracturing of the sill plates and studs at higher intensity levels. Nonstructural components, such as plumbing and HVAC systems, had the second most significant contribution, in the form of leaks and piping support failures, in the intensity range of interest. At higher intensities of shaking, losses due to residual drift became the second largest contributor to the total loss, reducing in some cases the apparent relative contributions of the other components because in this case the structure is taken as a total loss. When residual drifts exceed 1%, the building is deemed irreparable, producing a high contribution to the total seismic loss.

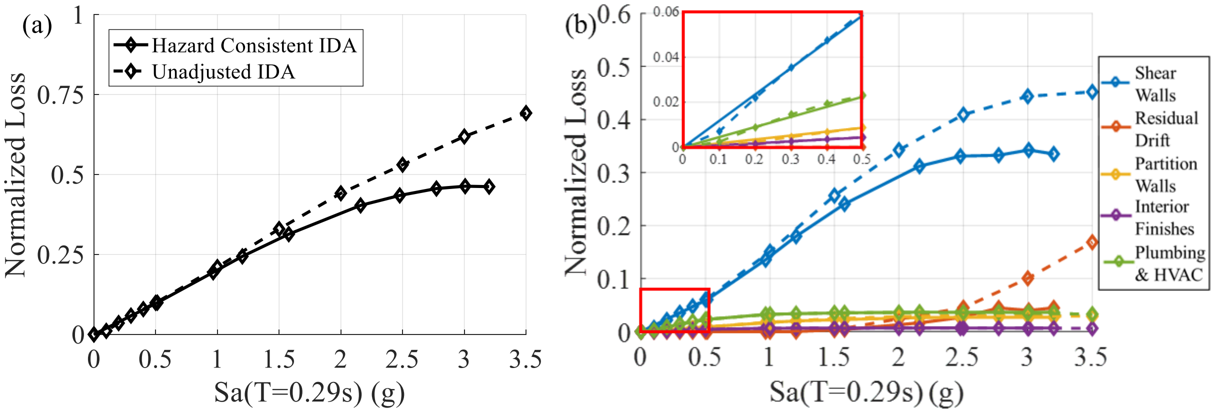

Figure 9. **Expected losses for the one-story building showing: a) total expected loss and b) breakdown of the total loss by component type.**

At lower intensities (*e.g., Sa(T₁)* <1.5g), the hazard consistent and unadjusted IDA provide similar results. In this range of intensities, the spectral shape (*SaRatio*) of the induced ground motion set is very close to the target *SaRatio*, and, because the structure is not responding significantly in the nonlinear range, results are not very dependent on *SaRatio*. However, at larger intensities, the hazard consistent IDA predicts lower losses. This trend occurs because the target *SaRatios* calculated in Table 2 are all larger than the mean of the induced record set, suggesting that the expected spectra is less damaging than those used in the analysis, so the adjustment to hazard consistency lowers the EDPs (Figure 8) and, as a result, losses (Figure 9).

Figure 10(a) shows the total expected seismic losses for the two-story building. For this two-story building, the total replacement cost is \$1.5 million. Figure 10(b) provides the deaggregation of the total losses by component category, which follows similar trends to those observed for the one-story building. At higher intensity levels (*e.g.*, *Sa(T₁)* > 1.5g), losses from residual drift became the highest contributor to the total loss. Residual drifts are much higher overall in the two-story model, due to the first-story's P-Δ driven response affected by loads in the upper story.

Losses in the one and two-story buildings are compared in Figure 11. The expected normalized seismic loss of the one-story building is higher than the two-story building at most hazard levels. In this range, drifts in the one-story building are very similar to the two-story building, but the variability in the drifts is greater due to differences in stiffness in the two orthogonal directions, producing slightly greater losses. For hazard levels more rare than 2.5×10^{-4} events/year, losses due to residual drift and collapse increase the potential losses for the two-story building. In particular, the higher seismic mass and multiple stories increases the chance for a first-story P-Δ driven collapse relative to the one-story building.

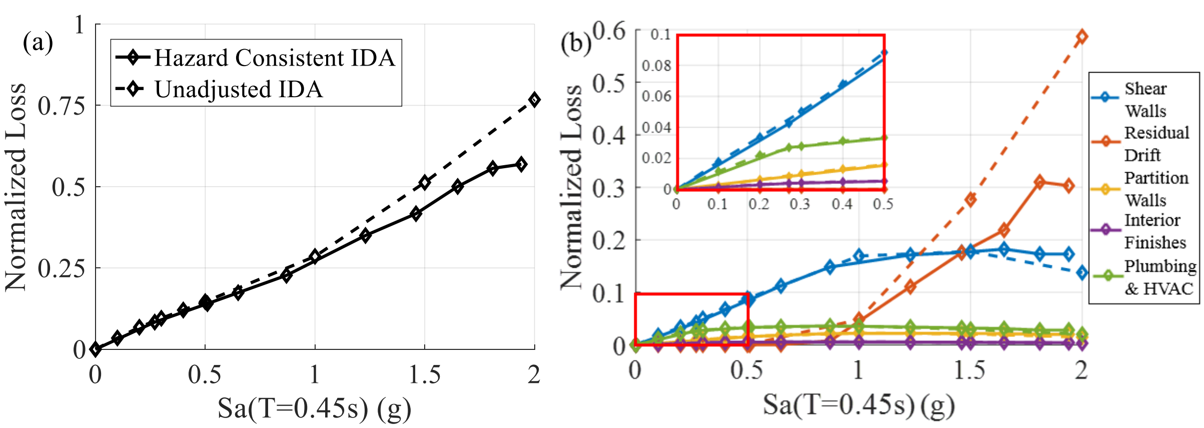

Figure 10. **Expected losses for the two-story building showing: a) total normalized loss and b) breakdown of the total loss by component type.**

We can compare the simulation results to damage observed in two recent earthquakes in Oklahoma: the 2016 M_W 5.8

Pawnee earthquake and 2016 M_W 5.0 Cushing earthquake. In the first event, the USGS estimated that Pawnee, OK experienced intensities between *Sa(0.3s)* = 0.28g and 0.35g [72]. The Cushing event was about three kilometers from Cushing, and the two closest stations, OK914 (<2 km from the epicenter) and OK915 (~3 km), reported Sa(0.3s) of 0.2g and 0.5g, respectively [73]. The damage reported to light-frame wood buildings in the two earthquakes was very similar. In the town of Pawnee and the bordering Pawnee Nation, damage included cracking to shear walls and partition walls, ceiling cracks, broken windows, foundation damage, brick chimney failure, and damage to exterior finishes, such as mortar deterioration and cracking, brick façade cracks and spalling, and awning damage [4, 74]. In Cushing, a reconnaissance team [73] reported "damage was limited to nonstructural components, mainly partition wall cracks in corners and near openings… There were few observed instances of structural damage to light frame wooden structures".

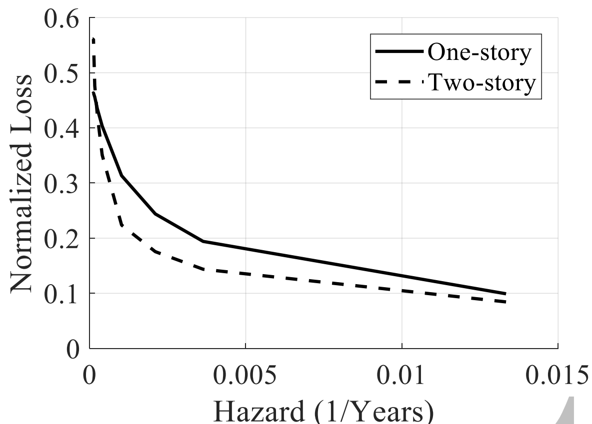

Figure 11. Expected losses for the one and two-story buildings.

Here, the observed damage to buildings in these earthquakes is compared to the results from our analysis. In Figure 12(a), expected seismic losses in the one-story building are superimposed with the USGS estimated intensities for the Pawnee earthquake in Pawnee, and the measured intensities in the Cushing earthquake. Our assessment predicts minor damage to the shear walls, plumbing, HVAC, and partition walls. For the same intensity range, Figure 12(b) shows the estimated percent of exterior shear walls in each DS (defined in Table 1), as calculated during the loss assessment using SP3. For the shaking intensities of interest in Pawnee, the model predicts that approximately 15 – 20% of the exterior shear walls are expected to be in DS 1, *i.e.* screws popping, minor cracking, etc., and a very small fraction of the shear walls would be expected to be in DS 2, *i.e.* moderate cracking or crashing of wallboards, or DS 3. Similarly, 10 – 27% of the exterior shear walls are expected to be in DS 1 if intensities similar to the Cushing earthquake are observed. These expected damage results agree reasonably well with the reported damage from the Pawnee and Cushing earthquakes. In Pawnee, the first four paid-out insurance claims (of more than 285) totaled $24,000, with the largest claim being $21,000 [75], or 15% of the insured value [76]. Our models, which are for modern code conforming buildings, *i.e.,* likely the best performers, are somewhat lower, with expected losses of 4-10%.

DAMAGE ACCUMULATION AND RESPONSE OF BUILDINGS IN SEQUENCES OF MOTIONS

We next examine damage and responses of the buildings from the two- and three-motion sequences. For the purposes of this discussion, we define damage accumulation as additional damage (*i.e.,* loss) that a building sustains in a second ground motion, compared to damage that is sustained from a ground motion of the same intensity when the building is undamaged (i.e., damage in the first motion). This accumulation, if it occurs, is the result of a reduction in capacity, or an increase in fragility, due to the pre-existing damage from the first motion.

Figure 13 provides the first set of insights into accumulating damage, comparing the average maximum SDR, as a function of Sa, for different levels of initial damage. SDR is used to investigate damage accumulation, as it is highly correlated with losses. When the building is initially damaged to DS4, the response subsequently is very close to the undamaged building; similar results (not shown) are observed for the lower DSs. However, a building that is initially damaged to DS5 or DS6 has a much different response in a second motion than the undamaged structure and showed some accumulation of damage in the following ground motion. This finding suggests that a building must be severely damaged in the prior event in order to significantly alter a building's fragility or losses in subsequent events. Figure 14 confirms these results, showing that the fragility curve for DS4 for the two-story building initially damaged to DS3 in a two-motion sequence is very similar to the DS4 curve for the undamaged building. Similar results are observed for the other building, and studies of other kinds of buildings, including concrete, steel, and light-frame wood, have also reached this conclusion, *e.g.* [47, 77, 50]. DS4 and higher have a low probability of being reached given the observed intensities in Oklahoma (Figure 12), suggesting that accumulation of fragility is unlikely for these structures. (Note that these results and those that follow do not consider the hazard consistent adjustments. Figure 9 and Figure 10 showed that the hazard consistent adjustments did not make significant changes at the more frequent intensities of the most interest, *i.e.* the lower end of the curve.)

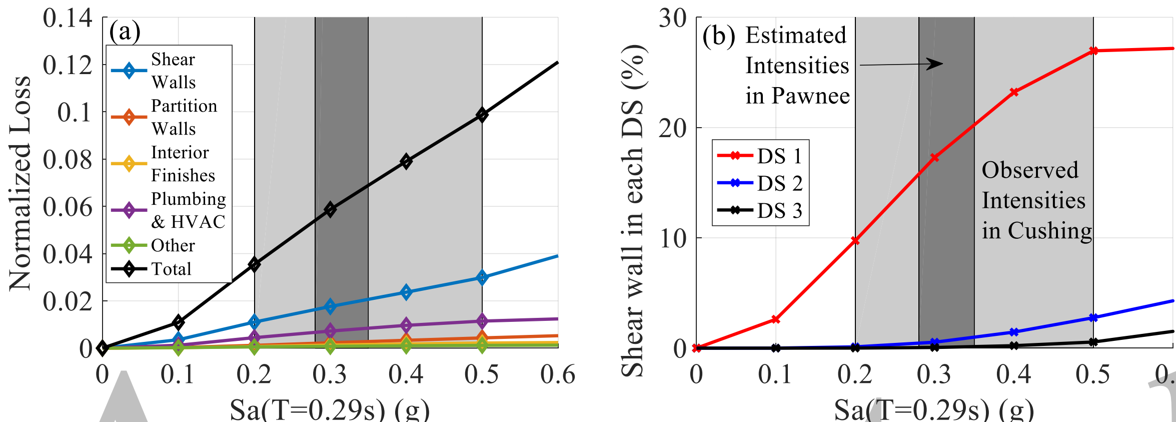

Figure 12. **Expected losses for the one-story building showing: a) breakdown of the total loss to quantify contributions from different types of components and b) percent of exterior shear walls in each damage state for the component, overlaid with estimated intensities observed in the Pawnee, OK Mw 5.8 and in the Cushing, OK Mw 5.0 Earthquakes.**

Figure 13 also compares the response from the two and three-motion sequences for different initial levels of damage. There is very little difference in building response between the two- and three-motion sequences. This trend was true for buildings initially damaged to DS1-6 and is consistent with other studies that found that the preceding DS was critical for subsequent response, but not the path to the DS, *e.g.,* [47]. As a result, we focus on results from two-motion sequences in the remainder of this section.

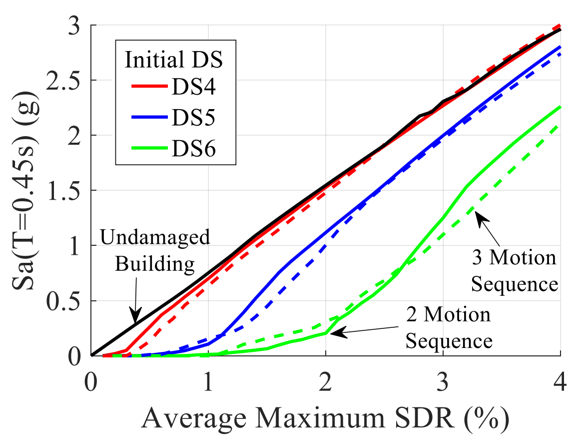

Figure 13. **Effects of initial damage on response of the two-story building, showing average maximum SDR for the last motion in the sequences, as a function of ground motion intensity.**

Figure 15(a) shows the expected losses for the one-story building in a two-motion sequence when the building is repaired at the end of the sequence, as a function of the ground motion intensity of the first and second motions. The symmetry of the surface about the horizontal axes shows that damage accumulation was not significant, because a second motion of the same intensity as a first motion causes the types of damage and, hence, the same repair actions and the same losses [17]. Thus, Figure 15(a) shows that expected losses are a function only of the maximum intensity observed, rather than the sequence of intensities. We do not observe damage accumulation because buildings need to be pushed deep into the nonlinear range in the first motion before their fragility to seismic loss in subsequent motions is significantly affected.

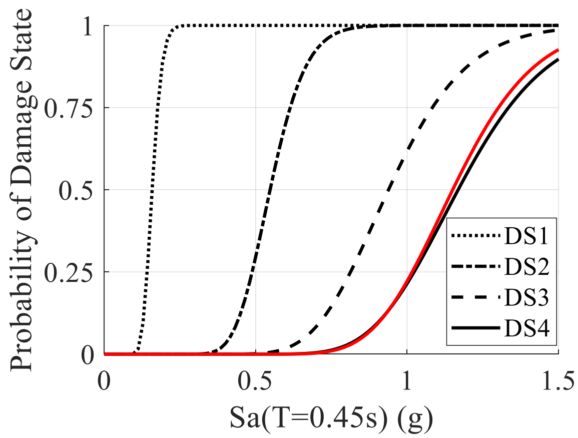

Figure 14. Fragility curves for the two-story building, showing the probability of reaching DSs 1-4, given $Sa(T_1)$. The red curve shows the DS 4 fragility the two-story building damaged to DS3 in motion 1 in a two-motion sequence.

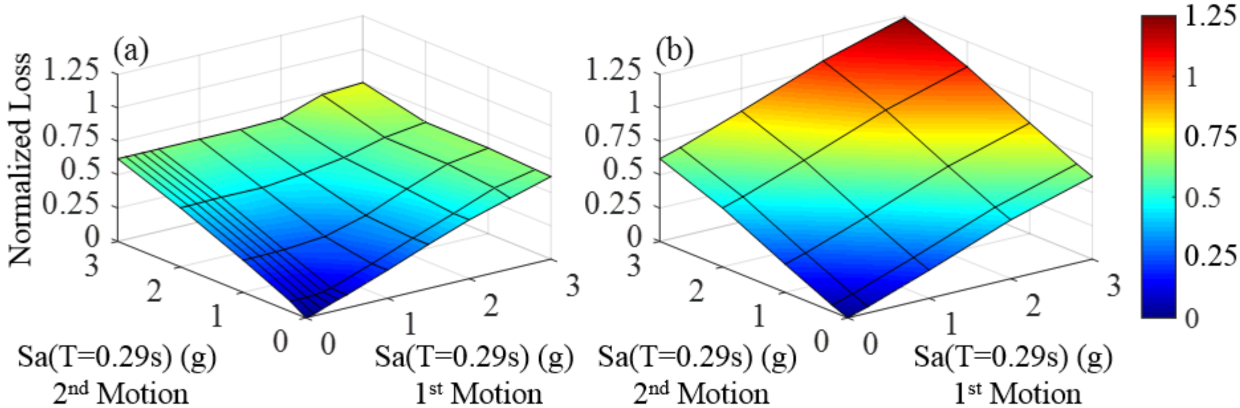

Figure 15. Expected loss for the one-story building subjected to two-motion sequences considering: a) repair at the end of the sequence and b) repair after each motion in the sequence.

However, the absence of damage accumulation by this definition does not mean that cracks in walls do not grow during subsequent motions in the sequence. Van de Lindt et al. [30] found that cracks in gypsum wallboard lengthened and widened in successive shaking events with similar maximum drift demands in a full-scale shake table test. To investigate in more detail how the second motion may be altering building damage in this study, Figure 16(a) shows an example two-motion sequence for the one-story building. This scenario was chosen because it is representative of a seismic sequence of two motions with similar intensities to those observed in the Cushing and Pawnee earthquakes. The largest drift (and loss corresponding to 7.4% of the building value) was reached in the first ground motion; this motion also has slightly larger spectral acceleration in the direction that dominates the drifts. The maximum response occurred in the first motion, so the total losses are unchanged (assuming the building is repaired after both motions), and the largest contributor to loss is determined to be the cracking of paint over fasteners or joints (totaling approximately $4000). For this same sequence, Figure 16(b) shows a damage index developed by Park and van de Lindt [78] for gypsum wallboard shear walls, calibrated to NEESWood experimental tests. This damage index is a function of the maximum drift during loading, the ultimate drift during monotonic loading, the yield drift, the absorbed hysteretic energy, and properties of the shear walls such as nail spacing and height-to-width ratio. As shown in Figure 16(b), the damage index for the building increases in the second motion, indicating that the structure is more damaged. This result is largely a function of the inclusion of absorbed hysteretic energy in the damage index, which increases when the second ground motion is also considered. Nevertheless, this result shows that damage is worsening in subsequent events, even though assessment of vulnerability and repair costs (losses) do not pick this up.

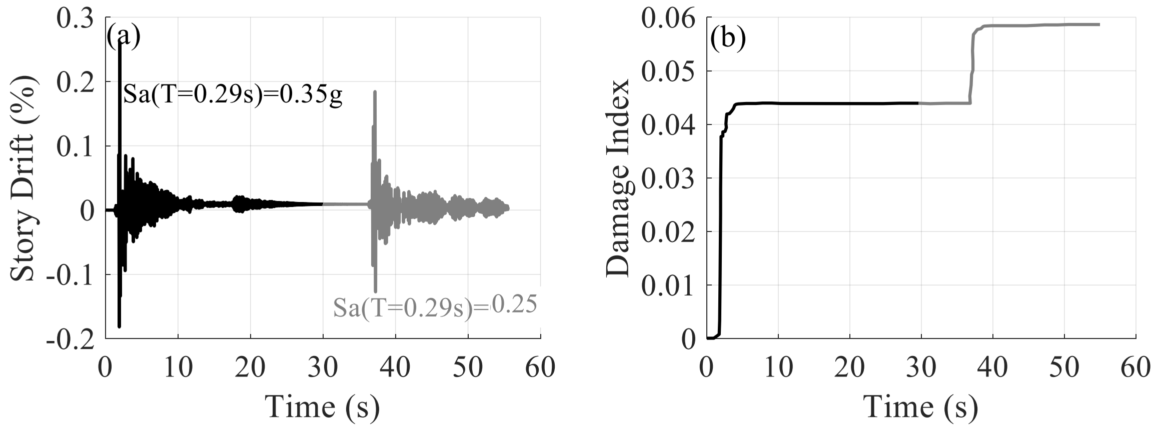

Figure 16. Example two-motion sequence, showing evolution of a) story drifts and b) the Park and van de Lindt [78] **damage index for the one-story building.**

These patterns appear to be consistent with residents' reports; as one respondent reported to the USGS 'Did you Feel it?' site, "there is a continuation of cracks in walls from previous large quakes. I have repaired them only to have new ones appear 6 months later when another quake hits" [14].To explore the impacts of these earthquakes on residents in more detail, Figure 15(b) shows the expected losses if the building were to be repaired (to its undamaged state) after each motion in the sequence. If the building is repaired after each earthquake, as might be expected, the losses are much higher than if the building is repaired just once after the sequences. Thus, even though existing damage is not amplifying fragility, homeowners affected by these sequences would be still be experiencing amplified seismic losses.

CONCLUSIONS

This study quantifies damage to and seismic losses for light-frame wood buildings when subjected to induced earthquakes like those experienced in Oklahoma and Kansas, which have to-date been small to moderate magnitudes, but sometimes occur in swarms. One and two-story multifamily wood frame buildings are investigated by dynamically simulating their seismic response using 3D nonlinear models that are subjected to recorded ground motion sequences from induced earthquakes. Damage is quantified through seismic losses, which are estimated using the FEMA P-58 methodology [17]. In order to avoid bias potentially created by scaling ground motions above the level they are recorded, the hazard-consistent incremental dynamic analysis methodology is employed. This methodology adjusts structural response and other parameters to reflect the dominant hazard contributors at a particular location.

Results show that at shaking levels experienced in recent earthquakes in Oklahoma and Kansas, minor damage, consisting of cracking of interior finishes and wallboards and damage to plumbing and HVAC systems is expected, which is consistent with observed damage in these recent earthquakes. These losses correspond to approximately 6% of the replacement value of the structure at the levels of shaking experienced.

When considering multiple earthquakes in a seismic sequence, damage and fragility did not seem to be accumulating. In other words, damage was typically light enough that it did not alter the capacity of the building to withstand the next event in the sequence. In addition, a second event did not change the estimated repair costs or seismic losses because the losses are driven solely by the maximum response in a sequence. This does not mean, though, that cracks are not growing or widening in a second event. We used the Park and van de Lindt [78] damage index to show that hysteretic energy absorption and damage are accumulating; these changes are just not significant enough to change peak responses and losses. In addition, the study shows that if repairs are implemented after each earthquake in the sequences, total seismic losses increase greatly, increasing the overall economic impact of these events. This choice of repair strategy is important for homeowners, who may not consider future earthquake events in decision making to repair current damages to their homes.

In this case, the use of the hazard consistent IDA methodology did not significantly alter the results. Although the spectra (frequency content) of the motions used in the assessment are highly peaked, the expected hazard in Edmond, Oklahoma is even more peaked. This hazard characteristic stems from the fact that we expect moderate magnitude close-in events to dominate the hazard at all levels.

ACKNOWLEDGMENTS

This material is based upon work supported by the National Science Foundation under Grant No. 1515438 to the Colorado Collaboratory for Induced Seismicity. Any opinion, findings, and conclusions or recommendations expressed in this material are those of the author(s) and do not necessarily reflect the views of the National Science Foundation. The authors would like to acknowledge the contributions of Greg Deierlein, Morgan Moschetti, and Kuanshi Zhong. We thank Ershad Ziaei Ghehnavieh and Weichiang Pang for sharing their models of wood light frame buildings, which were modified for SDC B in this study. This work utilized the RMACC Summit supercomputer, which is supported by the National Science Foundation (awards ACI-1532235 and ACI-1532236), the University of Colorado Boulder, and Colorado State University [79]. We appreciate the feedback on the manuscript from two anonymous reviewers and Dr. Mehmet Celebi.

REFERENCES

[1] M. Petersen, C. Mueller, M. M. P, S. Hoover, A. Llenos, W. Ellsworth, A. Michael, J. Rubinstein, A. McGarr and K. Rukstales, "Seismic-Hazard Forecast for 2016 Including Induced and Natural Earthquakes in the Central and Eastern United States," *Seismological Research Letters,* vol. 87, no. 6, pp. 1327-1341, 2016.

[2] T. Liu, N. Luco and A. Liel, "Increases in Life-Safety Risks to Building Occupants from Induced Earthquakes in the Central United States," *Earthquake Spectra,* p. In Press, 2018.

[3] M. Barba-Sevilla, B. Baird, A. Liel and K. Tiampo, "Hazard implications of the 2016 Mw 5.0 Cushing, OK earthquake from a joint analysis of damage and InSAR data," *Remote Sensing,* vol. 10, no. 11, p. 1715, 2018.

[4] A. Knife Chief, *Pawnee Executive Directior, Personal Correspondence,* 2017.

[5] USGS, "Earthquake Hazards Program - Earthquake Catalog," 8 March 2017. [Online]. Available: https://earthquake.usgs.gov/earthquakes/search/. [Accessed 1 March 2017].

[6] USGS, "Earthquake Statistics," 2017. [Online]. Available: https://earthquake.usgs.gov/earthquakes/browse/stats.php.

[7] OGS, "Oklahoma Earthquakes Magnitude 3.0 and greater," Oklahoma Geological Survey, 2018. [Online].

[8] K. Keranen, M. Weingarten, G. Abers, B. Bekins and S. Ge, "Sharp increase in central Oklahoma seismicity since 2008 induced by massive wastewater injection," *Science,* vol. 345, no. 6195, pp. 448-451, 2008.

[9] A. Llenos and A. Michael, "Modeling Earthquake Rate Changes in Oklahoma and Arkansas: Possible Signatures of Induced Seismicity," *Bulletin of the Seismological Society of America,* vol. 103, no. 5, pp. 2850-2861, 2013.

[10] UBC, "Uniform Building Code," International Conference of Building Officials, Whittier, California, 1997.

[11] ASCE, "Minimum Design Loads for Buildings and Other Structures," ASCE, Washington DC, 2010.

[12] A. Tracy and A. Javernick-Will, "Induced Seismicity Survey Results," University of Colorado Boulder, Boulder, 2018.

[13] Kansas Sierra Club, "Facebook - Kansas Sierra Club," 8 March 2017. [Online]. Available: https://www.facebook.com/KansasSierraClub/. [Accessed 1 March 2017].

[14] V. Quitoriano and D. Wald, *Personal Communication,* 2017.

[15] C. Trapasso, "Life in the Earthquake Capital of the U.S.: A Tale of Man-Made Disasters and Survival," 27 September 2017. [Online]. Available: https://www.realtor.com/news/trends/man-made-earthquakes-in-oklahoma/.

[16] S. Barrett, "The link between hydrofracking, wastewater injection and earthquakes: key issues for re/insurers," Swiss Reinsurance Company, 2016.

[17] FEMA, "FEMA P-58-1: Seismic Performance Assessment of Buildings. Volume 1–Methodology.," Federal Emergency Management Agency, Washington DC, 2012.

[18] M. Petersen, C. Mueller, M. Moschetti, S. Hoover, K. Rukstales, D. McNamara, R. Williams, A. Shumway, P. Powers, P. Earle, A. Llenos, A. Michael, J. Rubinstein, J. Norbeck and E. Cochran, "2018 One-Year Seismic Hazard Forecast for the Central and Eastern United States from Induced and Natural Earthquakes," *Seismological Research Letters,* vol. 89, no. 3, pp. 1049-1061, 2018.

[19] I. Grigoratos, P. Bazzurro, E. Rathje and A. Savvaidis, "A framework to quantify induced seismicity due to wastewater," in *Proceedings of the 11th National Conference in Earthquake Engineering*, Los Angeles, 2018.

[20] R. Schultz, R. Wang, Y. Gu, K. Haug and G. Atkinson, "A seismological overview of the induced earthquakes in the Duvernay play near Fox Creek, Alberta," *Journal of Geophysical Research: Solid Earth,* vol. 122, no. 1, pp. 492-505, 2017.

[21] J. Bommer, P. Stafford, B. Edwards, B. Dost, E. van Dedem, A. Rodriguez-Marek, P. Kruiver, J. van Elk, D. Doornhof and M. Ntinalexis, "Framework for a ground-motion model for induced seismic hazard and risk analysis in the Groningen gas field, the Netherlands," *Earthquake Spectra,* vol. 33, no. 2, pp. 481-498, 2017.

[22] R. Chase and A. Liel, "Effect of Ground Motions from Induced Earthquakes on Response of Brittle Structures," *Seismological Research Letters,* p. In preparation, 2018.

[23] R. Chase, "Structural Response and Risk Considering Regional Ground Motion Characteristics," Ph.D. Thesis, University of Colorado Boulder, 2018.

[24] S. Harvey, S. Heinrich and K. Muralleetharan, "A Framework for Post-Earthquake Response Planning in Emerging Seismic Regions: An Oklahoma Case Study," *Earthquake Spectra,* vol. 34, no. 2, pp. 503-525, 2018.

[25] F. Khosravikia, A. Potter, V. Prakhov, G. Zalachoris, T. Cheng, A. Tiwari, P. Clayton, B. Cox, E. Rathje, E. Williamson and J. Paine, "Seismic Vulnerability and Post-Event Actions for Texas Bridge Infrastructure," FHWA/TX-17/0-6916-1, Center for Transportation Research (CTR), 2018.

[26] B. Ellingwood, D. Rosowsky and W. Pang, "Performance of light-frame wood residential construction subjected to earthquakes in regions of moderate seismicity.," *Journal of Structural Engineering,* vol. 134, no. 8, pp. 1353-1363, 2008.

[27] C. Kircher, R. Reitherman, R. Whitman and C. Arnold, "Estimation of Earthquake Losses to Buildings," *Earthquake Spectra,* vol. 13, no. 4, pp. 703-720, 1997.

[28] B. Folz and A. Filiatrault, "Seismic analysis of woodframe structures. II: Model implementation and verification," *Journal of Structural Engineering,* vol. 130, no. 9, pp. 1361-1370, 2004.

[29] S. Pei, J. Van de Lindt, S. Pryor, H. Shimizu, H. Isoda and D. Rammer, "Seismic testing of a full-scale mid-rise building: The NEESWood Capstone Test," MCEER, 2010.

[30] J. van de Lindt, R. Gupta, S. Pei, K. Tachibana, Y. Araki, D. Rammer and H. Isoda, "Damage assessment of a full-scale six-story wood-frame building following triaxial shake table tests," *Journal of Performance of Constructed Facilities,* vol. 26, no. 1, pp. 17-25, 2010.

[31] A. Filiatrault, D. Fischer, B. Folz and C. Uang, "Seismic Testing of Two-Story Woodframe House: Influence of Wall Finish Materials," *Journal of Structural Engineering,* vol. 128, no. 10, pp. 1337-1345, 2002.

[32] I. Christovasilis, A. Filiatrault, M. Constantinou and A. Wanitkorkul, "Incremental Dynamic Analysis of Woodframe Buildings," *Earthquake Engineering and Structural Dynamics,* vol. 38, no. 4, pp. 477-496, 2009.

[33] ATC, "Solutions to the Issues of Short-Period Building Seismic Performance," ATC, 2018. [Online]. Available: https://www.atcouncil.org/projects/projects-active. [Accessed November 2017].

[34] C. Kircher, W. Pang, E. Ziaei, A. Filiatrualt and S. Schiff, "Solutions to the Short-Period Building Performance Paradox: A Focus on Light-Frame Wood Buildings," in *SEAOC Convention*, Maui, 2016.

[35] B. Folz and A. Filiatrault, "Cyclic analysis of wood shear walls," *Journal of Structural Engineering,* vol. 127, no. 4, pp. 433-441, 2001.

[36] B. Folz and A. Filiatrault, "A computer program for seismic analysis of woodframe structures," Consortium of Universities for Research in Earthquake Engineering, Richmond, California, 2004.

[37] J. van de Lindt, S. Pei, H. Liu and A. Filiatrault, "Three-dimensional seismic response of a full-scale light-frame wood building: Numerical study," *Journal of Structural Engineering,* vol. 136, no. 1, pp. 56-65, 2009.

[38] W. Pang, E. Ziaei and A. Filiatrault, "A 3D Model for Collapse Analysis of Soft-story Light-frame Wood Buildings," in *World Conference on Timber Engineering*, Auckland, NZ, 2012.

[39] L. Decanini, C. Gavarini and F. Mollaioli, "Some remarks on the Umbria-Marche earthquakes of 1997," *European Earthquake Engineering,* vol. 14, no. 3, pp. 18-48, 2000.

[40] M. Çelebi, P. Bazzurro, L. Chiaraluce, P. Clemente, L. Decanini, A. DeSortis, W. Ellsworth, A. Gorini, E. Kalkan, S. Marcucci and G. Milana, "Recorded motions of the 6 April 2009 Mw 6.3 L'Aquila, Italy, earthquake and implications for building structural damage: overview," *Earthquake Spectra,* vol. 26, no. 3, pp. 651-684, 2010.

[41] G. Ballio and C. Castiglioni, "An approach to the seismic design of steel structures based on cumulative damage criteria," *Earthquake Engineering & Structural Dynamics,* vol. 23, no. 9, pp. 969-986, 1994.

[42] C. Amadio, M. Fragiacomo and S. Rajgelj, "The effects of repeated earthquake ground motions on the non-linear response of SDOF systems," *Earthquake Engineering & Structural Dynamics,* vol. 32, no. 2, p. 291–308, 2003.

[43] J. Ghosh, J. Padgett and M. Sánchez-Silva, "Seismic damage accumulation in highway bridges in earthquake-prone regions," *Earthquake Spectra,* vol. 31, no. 1, pp. 115-135, 2015.

[44] Y. Park and A. Ang, "Mechanistic seismic damage model for reinforced concrete," *Journal of Structural Engineering,* vol. 111, no. 4, pp. 722-739, 1985.

[45] F. Jalayer and H. Ebrahimian, "Seismic risk assessment considering cumulative damage due to aftershocks," *Earthquake Engineering & Structural Dynamics,* vol. 46, no. 3, pp. 369-389, 2017.

[46] G. Hatzigeorgiou and A. Liolios, "Nonlinear behaviour of RC frames under repeated strong ground motions," *Soil Dynamics and Earthquake Engineering,* vol. 30, no. 10, pp. 1010-1025, 2010.

[47] M. Raghunandan, A. B. Liel and N. Luco, "Aftershock collapse vulnerability assessment of reinforced concrete frame structures," *Earthquake Engineering & Structural Dynamics,* vol. 44, no. 3, pp. 419-439, 2015.

[48] S. Tesfamariam, K. Goda and G. Mondal, "Seismic vulnerability of reinforced concrete frame with unreinforced masonry infill due to main shock–aftershock earthquake sequences," *Earthquake Spectra,* vol. 31, no. 3, pp. 427-1449, 2015.

[49] M. Shokrabadi and H. Burton, "Risk-based assessment of aftershock and mainshock-aftershock seismic performance of reinforced concrete frames," *Structural Safety,* vol. 73, pp. 64-74, 2018.

[50] N. Nazari, J. van De Lindt and Y. Li, "Effect of mainshock-aftershock sequences on woodframe building damage fragilities," *Journal of Performance of Constructed Facilities,* vol. 29, no. 1, p. 04014036, 2013.

[51] K. Goda and M. Salami, "Inelastic seismic demand estimation of wood-frame houses subjected to mainshock-aftershock sequences," *Bulletin of Earthquake Engineering,* vol. 12, no. 2, pp. 855-874, 2014.

[52] S. Rennolet, M. Moschetti, E. Thompson and W. Yeck, "A Flatfile of Ground Motion Intensity Measurements from Induced Earthquakes in Oklahoma and Kansas," *Earthquake Spectra,* vol. 34, no. 1, pp. 1-20, 2018.

[53] T. D. Ancheta, R. B. Darragh, J. P. Stewart, E. Seyhan, W. J. Silva, B. S. Chiou, K. E. Wooddell, R. W. Graves, A. R. Kottke and D. M. Boore, "PEER NGA-West2 Database," Pacific Engineering Research Center, Berkeley, CA, 2013.

[54] J. Ruiz-Garcia and J. C. Negrete-Manriquez, "Evaluation of drift demands in existing steel frames under as-recorded far-field and near-fault mainshock–aftershock seismic sequences," *Engineering Structures,* vol. 33, no. 2, pp. 621-634, 2011.

[55] L. Eads, E. Miranda and D. Lignos, "Spectral shape metrics and structural collapse potential.," *Earthquake Engineering & Structural Dynamics,* vol. 45, no. 10, pp. 1643-1659, 2016.

[56] FEMA, "FEMA P-695 Quantification of Building Seismic Performance Factors," Federal Emergency Management Agency, Washington DC, 2009.

[57] Authentic Custom Homes, Homes by Taber LLC, Silver Custom Homes and Sun Custom Homes, *Typical siding in Oklahoma,* Oklahoma, 2018.

[58] W. Pang and S. Shirazi, "Corotational Model for Cyclic Analysis of Light-frame Wood Shear Walls and Diaphragms," *ASCE Journal of Structural Engineering, Special issue NEES 2: Advances in Earthquake Engineering,* vol. 139, no. 8, pp. 1303-1317, 2013.

[59] S. Pei and J. van de Lindt, "“Seismic numerical modeling of a six-story light-frame wood building: Comparison with experiments," *Journal of Earthquake Engineering,* vol. 15, no. 6, pp. 924-941, 2011.

[60] R. Chandramohan, J. Baker and G. Deierlein, "Quantifying the influence of ground motion duration on structural collapse capacity using spectrally equivalent records," *Earthquake Spectra,* vol. 32, no. 2, p. 927–950, 2016.

[61] M. Raghunandan and A. Liel, "Effect of ground motion duration on earthquake-induced structural collapse," *Structural Safety,* vol. 41, pp. 119-133, 2013.

[62] S. Mahin, "Effects of duration and aftershocks on inelastic design earthquakes," in *Proceedings of the Seventh World Conference on Earthquake Engineering*, Instanbul, 1980.

[63] E. Ziaei Ghehnavieh, "Seismic Analysis of Light-Frame Wood Building with a Soft-Story Deficiency," PHD Thesis, Clemson University, 2017.

[64] A. Koliou, A. Filiatrault and A. Kircher, "Assessing Modeling Complexities on the Seismic Performance of an Instrumented Short-Period Hospital," *Journal of Performance of Constructed Facilities,* vol. 31, no. 1, p. 04016078, 2016.

[65] Haselton Baker Risk Group, "Seismic Performance Prediction Program," 2018. [Online]. Available: www.hbrisk.com.

[66] D. Vamvatsikos and C. A. Cornell, "Incremental Dynamic Analysis," *Eathquake Engineering & Structural Dynamics,* vol. 31, no. 3, pp. 491-514, 2002.

[67] J. Baker and C. Cornell, "Spectral shape, epsilon and record selection," *Earthquake Engineering & Structural Dynamics,* vol. 35, no. 9, pp. 1077-1095, 2006.

[68] R. Chandramohan, "Duration of earthquake ground motion: Influence on structural collapse risk and integration in design and assessment practice.," PhD. Thesis, Stanford University, 2016.

[69] M. Petersen and A. Shumway, *Personal Communication,* 2018.

[70] G. Atkinson, "Ground-motion prediction equation for small-to-moderate events at short hypocentral distances, with application to induced-seismicity hazards," *Bulletin of the Seismological Society of America,* vol. 105, no. 2A, pp. 981-992, 2015.

[71] K. Zhong and G. Deierlein, *Personal Communication,* 2018.

[72] USGS, "M 5.8 - 14km NW of Pawnee, Oklahoma," 3 September 2016. [Online]. Available: https://earthquake.usgs.gov/earthquakes/eventpage/us10006jxs#shakemap.

[73] J. Taylor, M. Celebi, A. Greer, E. Jampole, A. Masroor, S. Melton, D. Norton, N. Paul, E. Wilson and Y. Xiao, "EERI Earthquake Reconnaissance Team Report: M5.0 Cushing, Oklahoma, USA Earthquake on November 7, 2016," Earthquake Engineering Research Institute, Oakland, CA, 2017.

[74] B. Sewell, *Pawnee Mayor, Personal Communication,* 2017.

[75] C. Jones, "Record 5.8 Pawnee earthquake prompts more than 285 insurance claims for losses so far," 20 December 2016. [Online]. Available: https://www.tulsaworld.com/earthquakes/record-pawnee-earthquake-prompts-more-than-insurance-claims-for-losses/article_a60f902d-1ecf-5bcb-a0cd-5af5a3ee1c10.html.

[76] Oklahoma Insurance Commisson, *Oklahoma Earthquake Insurance Data,* Oklahoma, 2017.

[77] Q. Li and B. Ellingwood, "Performance evaluation and damage assessment of steel frame buildings under main shock–aftershock earthquake sequences," *Earthquake Engineering & Structural Dynamics,* vol. 36, no. 3, pp. 405-427, 2007.

[78] S. Park and J. van de Lindt, "Formulation of seismic fragilities for a wood-frame building based on visually determined damage indexes.," *Journal of Performance of Constructed Facilities,* vol. 23, no. 5, pp. 346-352, 2009.

[79] J. Anderson, P. Burns, D. Milroy, P. Ruprecht, T. Hauser and H. Siegel, "Deploying RMACC Summit: An HPC Resource for the Rocky Mountain Region," in *Proceedings of PEARC17*, New Orleans, 2017.